NON-INVASIVE MELANOMA DIAGNOSIS USING MULTISPECTRAL IMAGING

Ianisse Quinzán Suárez[1], Pedro Latorre Carmona[1], Pedro García Sevilla[1], Enrique Boldo[2], Filiberto Pla[1], Vicente García Jiménez[1], Rafael Lozoya[2] and Guillermo Pérez de Lucía[2]
[1]*Institute of New Imaging Technologies, Jaume I University, Castellón, Spain*
[2]*Fundación de la Comunidad Valenciana, Hospital Provincial de Castellón, Castellón, Spain*

Keywords: Melanoma detection, Multispectral images, Support Vector Machines, Class imbalance, SMOTE.

Abstract: The early analysis of pigmented skin lesions is important for clinicians in order to recognize malignant melanoma. However, it is difficult to differentiate it from benign skin lesions due to their similarity based on their appearance. Since melanoma has a tendency to grow inside the skin and the depth of penetration of light into the skin is wavelength dependent, a multispectral imaging acquisition and processing approach to classify pigmented lesions as melanoma seems appropriate. This paper presents a method to diagnose melanoma lesions over a group of 26 samples acquired with a multispectral system, where 6 of them are melanomas, and the other 20 are other types of pigmented lesions. A Leave-One-Out strategy is used to create the training/test set. The classification imbalance problem inherent to this dataset is alleviated using a $SMOTE$ technique. The random component of the $SMOTE$ methodology is dealt with running it 25 times and a Qualified Majority Voting (QMV) scheme is used to do the final classification, using SVM. Results show this strategy allows to obtain competitive classification quality results.

1 INTRODUCTION

Melanoma is becoming an important health problem worldwide. Just in Europe, 32107 cases for men and 35324 cases for women were detected in 2008, which represents an *Age Standardized Rate (European)* per 100000 of 11.5 and 11.4, respectively (ECO, 2011). Similar statistics appear in the United States (Jemal et al., 2010).

The current procedure for the detection of skin cancers in general is a clinical examination followed by a tissue biopsy and histopathology. However, there are several limitations associated to the process, and a recent clinical study showed that approximately 40% of suspicious biopsied lesions were classified as benign by pathologists (Mogensen and Jemec, 2007). Therefore, there is an urgent need for a real-time, non-invasive diagnostic method that can reduce morbidity and mortality for these cancers.

On the other hand, it is also crucial to diagnose melanoma early in its evolution, because it has been proven that its prognosis is directly related to the depth of the *lesion*. The first attempts to make an early diagnosis a reality came in 1985 with the *ABCD* diagnosis procedure (Friedman et al., 1985; Rigel and Friedman, 1993). Later, Abbasi (Abbasi et al., 2004) revised this procedure adding a new parameter, *E* of Evolving. Incorporation of the *ABCD* methodology into the evaluation campaigns was made in the mid 1980*s*. Since then, mass screenings have been undertaken. In the 1990*s* light-based visual technologies were incorporated to augment the early diagnosis capability.

The depth of penetration of light into the skin is wavelength dependent (Rigel et al., 2010). Information found at different depths is useful in order to differentiate benign pigmented skin lesions from malignant lesions. Here lies the potential to use multispectral imaging systems as noninvasive methods to help distinguish melanoma from other lesions.

Traditionally, multispectral imaging systems have been used in the field of remote sensing images of the Earth taken from satellites, but this technology is increasingly being introduced in other application fields such as medicine, biology, and art, among others.

Medicine, and particularly dermatology, seems to be a *natural* application field, because it can provide tools of special interest for new types of diagnostic tests and control treatments. It also has the advantage that the necessary data acquisition application is fast,

Quinzán Suárez I., Latorre Carmona P., García Sevilla P., Boldo E., Pla F., García Jiménez V., Lozoya R. and Pérez de Lucía G..
NON-INVASIVE MELANOMA DIAGNOSIS USING MULTISPECTRAL IMAGING.
DOI: 10.5220/0003843803860393
In *Proceedings of the 1st International Conference on Pattern Recognition Applications and Methods* (PRARSHIA-2012), pages 386-393
ISBN: 978-989-8425-98-0

simple and, above all, non-invasive. Besides, multispectral images, in fact, may give us useful information that can not be found in other parts of the wavelength spectrum.

The aim of this paper is to present a method to diagnose melanoma lesions over a group of samples acquired with a multispectral system, where there is a class imbalance problem alleviated using a technique called *SMOTE* (Chawla et al., 2002). The structure of the paper is as follows: Section 2 describes the sate of the art in the diagnosis of melanoma and other pigmented skin lesions. Section 3 explains multispectral image acquisition and processing tools used. Section 4 explains the classification method used and the *SMOTE* technique, and results and discussion are presented in Section 5. Conclusions are given in Section 6.

2 MELANOMA DIAGNOSIS

As stated in Section 1, early melanoma detection has traditionally been based on the *ABCD*/*ABCDE* systems, which provide a set of standards to facilitate visual recognition of these tumors. *ABCDE* stands for:

- A. Asymmetry: Melanoma lesions are typically irregular (asymmetric), benign moles are usually circular (symmetrical).
- B. Border: Melanoma lesions often have irregular edges, whereas benign moles have smooth edges.
- C. Colour: Injuries have many brown and black textured shapes. In the case of benign moles, usually only a brown spot appears.
- D. Diameter: Typically more than 6 millimeters in diameter. The diameter in the case of moles is usually much lower.
- E. Evolving: Comparison of the evolution of the lesion with time.

However, in the early stages of melanoma the above features are hardly visible and can lead to misdiagnosis. There have been various attempts to automatically obtain the *ABCD* characteristics. The first problem in these systems is the segmentation accuracy (Carrara et al., 2005). Once the image has been segmented, both morphological (Binder et al., 1998) as well as texture features (Deshabhoina et al., 2003) have been used. Segmentation following the *ABCD* rules has been done on grey scale images as well as for each band in multispectral images (Tomatis et al., 2003).

In the last decade, melanoma detection has included other parameters of study apart from the *ABCD* criteria, for example colour and spectral information. Cheng (Cheng et al., 2008) extracted a group of 17 features, the first 2 of geometric type, and the rest related to a *relative colour space* made subtracting the average (R,G,B) values of the normal skin from the corresponding values of the lesion image. After this, colour parameters related to the mean colour and its standard deviation, as well as skewness, energy and entropy, were assessed. R. Joe Stanley (Stanley et al., 2007) also used a classification strategy based on using a *relative colour space*. In this case, they *built* a colour histogram based on this space and classified the lesion as melanoma or non-melanoma depending on the percentage of pixels considered as melanoma. A pixel is considered as melanoma if it falls in the same histogram area where training melanoma pixels are located. On the other hand, Stoecker (Stoecker et al., 2011) used texture measures obtained from the co-occurrence matrix and color features based on the *RGB* and *XYZ* colour spaces (and their corresponding *normalized* versions). Tenenhaus (Tenenhaus et al., 2010) developed a method to classify images as melanoma or non-melanoma lesions under uncontrolled illumination conditions creating a 47 dimensional vector, formed by 5 geometric and 42 colorimetric features. The geometric features were obtained using a multiscale classification scheme, mimicking dermatologists' approach who first look at the image as a whole and then concentrate on local details to precisely localize the border.

Kuzmina (Kuzmina et al., 2011a; Kuzmina et al., 2011b) developed a system consisting of a Nuance *EX* (*CRi*) multispectral camera that acquired images in the $[450,950]$nm spectral range using an internal liquid crystal polarizer and three halogen lamps surrounding the surface to be imaged. After image acquisition and using a three-chromophore absorption (regression) model they obtained the relative concentrations of oxy-hemoglobin, deoxy-hemoglobin and melanin and considering the feature space of deoxy-hemoglobin and melanin, they classified lesions as melanoma or non-melanoma. Diebele (Diebele et al., 2011) proposed a *melanoma differentiation parameter* based on the different behaviour of melanoma from other lesions in terms of the Optical Density (*OD*) value at 540, 650 and 950nm, using the acquisition system proposed in (Kuzmina et al., 2011a; Kuzmina et al., 2011b).

Garcia−Uribe (Uribe et al., 2011) developed an oblique incidence diffuse reflectance spectrometer to conduct *in-vivo* measurements of the optical properties of three different types of pigmented skin lesions (melanoma, dysplastic and common nevi). Both

absorption and reduced scattering coefficient spectra were estimated from the images acquired in the $[455,765]$nm range for 144 pigmented skin lesions including 16 melanomas. Obtaining the extinction coefficients of oxy-hermoglobin, deoxy-hemoglobin and melanin allows to assess the total concentration of hemoglobin and the oxygen saturation, using this last figure as classification criteria for melanoma detection.

Sorg (Sorg et al., 2005) used hyperspectral imaging to study oxygen transportation using red fluorescent protein (RFP) to identify all tumor cells and green fluorescent protein (GFP) to identify hypoxic cells. In this way, maps were created, and (using hemoglobin saturation) were able to classify each pixel in the image as tumor cells (where only find RFP) or hypoxic tumor cells (where they find RFP and GFP).

Rajaram (Rajaram et al., 2010) used a CCD camera, a xenon lamp for white illumination, a pulsed nitrogen laser at 337nm, and a pulsed nitrogen laser at 445nm for melanoma detection. White illumination was used in combination with a model of diffuse reflectance spectroscopy to obtain parameters related to the morphology of the tissue under analysis. Laser illumination at 337 and at 445nm was used to activate two components ($NADH$ and FAD) which are related to the tissue metabolic activity.

Mazzoli (Mazzoli et al., 2010) used a camera modified to contain a LED lighting system able to acquire images at 950nm and a Monte-Carlo simulator able to infer the depth of the lesion from the acquired images (at 950nm).

Nagaoka (Nagaoka et al., 2011) developed a hyperspectral imaging system using an imaging spectrograph (ImSpector $V8E$, Specim) and a CCD camera (iXon) with a 1.3nm step width resolution, covering the $[380,780]$nm interval. Melanoma detection was obtained assessing the *spectral angle* between the spectral curve corresponding to normal skin and the curve of the skin lesion. From this angle, a probability distribution was assessed and used as the *melanoma discrimination index*. In particular, statistically significant differences between the melanoma and non-melanoma groups were analyzed using the Mann$-$Whitney $U-$ test.

Dhawan (Dhawan et al., 2005) developed an optical imaging system based on multispectral transillumination to provide images of skin lesions showing sub-surface pigmentation and vascular architecture based blood volume information, comparing their method with the Epiluminescence Light Microscopy method. Melanoma detection was made using image segmentation techniques based on the $CIE-L^*a^*b^*$ colour space.

Raposio (Raposio and et. al, 2007) developed a system for the detection of melanoma using a multispectral linear camera that acquired images in the $[400,1000]$nm range. They applied Principal Component Analysis (PCA) to the image and selected the first component. Then they assessed the local minima of the image histogram and used them as threshold values to segment the different image regions.

Melanoma detection is currently made not only using colour cameras or multispectral or hyperspectral systems. New fields of research are being opened in ultrasound imaging, $mRNA-$based signature, and electrical bioimpedance. For a complete survey of current and new commercial and non-commercial systems used the reader is referred to Table 1 (and details therein) of (Rigel et al., 2010).

3 IMAGE ACQUISITION

A set of two systems, consisting of two different cameras and two different Liquid Crystal Tunable Filters ($LCTF$) were used to acquire the multispectral images of the patients' skin lesions. Since they are tunable, the number of wavebands can be changed. A spectral resolution of 10nm was fixed. The use of the two filters is justified in order to cover the wavelength range from 400nm to 1100nm, and the use of the two cameras avoids the need to remove the filter from the camera to cover the whole wavelength range. The first camera was a CCD QImaging Retiga EX camera (12-bit, Monochrome Cooled camera without IR Filter). The sensor resolution is 1036×1360, down-sampled to 516×676 pixels. The second camera was a Marlin $F080B$ model. The VIS filter was attached to the Marlin camera, covering the $[400,720]$nm spectral range. The NIR filter was attached to the QImaging camera and it covered the $[650,1100]$nm range (see Figure 1). In both cases, a Canon TV zoom lens (whose focal distance varies between 8 and 48mm) was used before the filter, and a Macro Schneider system (SCHNEIDER, 2011) was used between the filter and the camera.

The illumination system was a Fiber-Lite $DC-950$ system (Dolan$-$Jenner industries) with a 150W Quartz halogen lamp, and a 3250° Kelvin colour temperature, connected to the camera optics through a fiber optic ring light guide. A white cylinder was attached to the optical ring. This was done in order to homogenize and concentrate light, significantly decreasing the exposure times required for each spectral band. It also controlled the distance between the camera and the lesion and prevented external light coming

Figure 1: Hardware for image acquisition.

into. The cylinder was 20cm long and 7.5cm in diameter. At 20cm distance, an approximately $8 \cdot 8$ cm^2 square Field-of-View was achieved.

3.1 Camera Calibration

The acquisition time per band used for the *LCTF* filters was obtained using an *ideal* reflectance diffuser object, called *spectralon*, which is built to reflect the same amount of light in the whole wavelength spectrum. This time was adjusted so that the image acquired of the spectralon were the same for all the image pixels and for all bands.

In order to accomplish this aim, an automatic calibration method was implemented. For one band, the acquisition time and grey level value are considered to increase linearly, if illumination and distance to object do not vary. The method consists of looking for two $(time, greylevel)$ pairs not allocated at extreme values, and then the exposure time is assessed based on the linear relationship assumed for an expected grey value.

3.2 Image Registration

Image registration is the process to obtain a *mapping* that allows one image to be superimposed over another image. Multispectral image acquisition is time consuming, because an image per band has to be acquired. During this time interval, involuntary movements of the patient may happen, and therefore image registration among spectral bands is a requirement. A method based on the maximization of the mutual information between two images (Maes et al., 1997) (Pluim et al., 2003) was applied. In particular, let us consider two images, A and B, of size $(M+1)\cdot(N+1)$ pixels. Registering image B against A can be done maximizing the following information criterion:

$$I(A,\widetilde{B}) = \sum_a \sum_b \widetilde{p}(a,b) \cdot \log \frac{\widetilde{p}(a,b)}{p(a) \cdot p(b)} \qquad (1)$$

where:

$$\widetilde{p}(a,b) = \frac{1}{M \cdot N} \sum_x \sum_y \delta(a, A(x,y)) \cdot \delta(b, \widetilde{B}(x,y)) \quad (2)$$

where $\widetilde{B}$ is the transformed version of B, a and b are the possible grey level values of the image and x and y, the pixel positions. δ is the *delta* function. $p(a,b)$ is the joint probability distribution of the grey levels of both images, and $p(a)$ ($p(b)$) is the probability distributions grey level a (b). The maximization of the mutual information was achieved using the *SIMPLEX* method (Press et al., 1992).

4 CLASSIFICATION

Multispectral image datasets related to melanoma classification are intrinsically high dimensional and low cardinality spaces where one of the classes (melanoma) usually contains a lower number of samples than the others. Therefore, solving this problem has to account for the relationships between the number of data points and the dimensionality of the feature spaces, on the one hand, and on the imbalance among the classes, on the other hand.

4.1 Support Vector Machines

Support Vector Machines (*SVMs*) is a classification technique that is considered robust *against* datasets of high dimensionality and low cardinality (Chang et al., 1999). Given a labeled training data set $\{(\mathbf{x}_1, y_1), \ldots, (bfx_n, y_n)\}$, where $\mathbf{x}_i \in R^N$ and $y_i \in \{-1, +1\}$ and a nonlinear mapping f, usually to a higher dimensional space, $f : R^N \rightarrow \mathcal{H}$, the SVM method solves:

$$\min_{\mathbf{w},\xi_i,b} \{\frac{1}{2}\|\mathbf{w}\|^2 + C\sum_i \xi_i\} \qquad (3)$$

constrained to:

$$y_i \cdot (\langle f(\mathbf{x}_i), \mathbf{w}\rangle + b) \geq 1 - \xi_i \quad \forall i = 1, \ldots, n \quad (4)$$

$$\xi_i \geq 0 \quad \forall i = 1, \ldots, n \qquad (5)$$

where w and b define a linear classifier in the feature space. Transformation f is assessed in such a way that the classification in the higher (transformed) dimensional space may be easier. The regularization parameter C controls the generalization capability of the classifier, and ξ_i are positive variables controlling the permitted errors.

4.2 Class Imbalance

Class imbalance constitutes one of the problems that has recently received most attention in research areas such as Machine Learning, Pattern Recognition

and Data Mining (Fernández et al., 2011). A two-class data set is said to be imbalanced if one of the classes (the minority one) is represented by a very small number of instances in comparison to the other (the majority) class (He and Garcia, 2009). It has been observed that class imbalance often leads to poor classification performance, especially for the minority classes because these are often biased towards the majority class. This issue is particularly important in real-world applications where it is costly to misclassify examples of the minority class.

Data level methods have been developed for dealing with the class imbalance problem. These methods consist of balancing the original data set, either by over-sampling the minority class and/or by under-sampling the majority class until the problem classes are approximately equally represented. Both strategies can be applied in any learning system since they act as a preprocessing phase, thus allowing the system to receive the training instances as if they belonged to a well-balanced data set. By using this strategy, any bias of the learning system towards the majority class due to the skewed class priors will hopefully be eliminated.

Several researchers have reported that over-sampling in general obtains more accurate results than the under-sampling methods (Batista et al., 2004), (He et al., 2005), (Hulse et al., 2007). The simplest method to increase the size of the minority class corresponds to random over-sampling, that is, a non-heuristic method that balances the class distribution through the random replication of positive examples. Nevertheless, since this method replicates existing examples in the minority class, overfitting is more likely to occur. Chawla et al (Chawla et al., 2002) proposed an over-sampling technique that generates new synthetic minority samples by interpolating between several preexisting positive examples that lie close together. It first finds the k nearest neighbors (k-NN) belonging to the minority class for each positive example and then, the synthetic examples are generated in the direction of some or all of the nearest neighbors. This method, called *Synthetic Minority Over-sampling TEchnique* (SMOTE), allows the classifier to build larger decision regions that contain nearby samples from the minority class. Depending upon the amount of over sampling required, neighbors from the k nearest neighbors are randomly chosen. Synthetic prototypes are generated in the following way: take the difference between the feature vector (instance) under consideration and its nearest neighbor. Multiply this difference by a random number between 0 and 1, and add it into the feature vector under consideration.

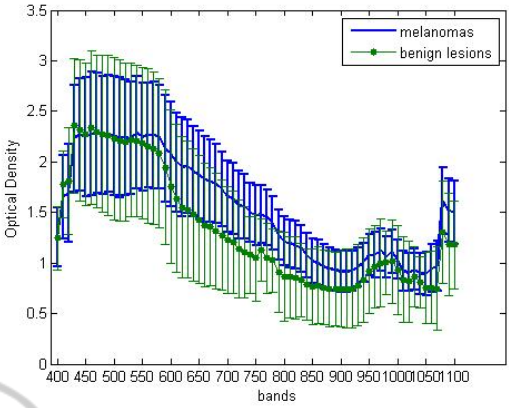

Figure 2: Optical Density curves of melanoma and a pigmented benign lesion.

5 EXPERIMENTAL RESULTS

A group of 26 samples (each one with the two available *VIS* and *NIR* components) of skin lesions was acquired by the multispectral system. All of them were preliminary classified as suspected pigmented lesions, and all of them were biopsied. Biopsy determined that 6 of them were melanoma and the other 20 were other types of lesions.

For each lesion, a region of interest was manually selected, and the mean value (normalized between 0 and 1) for that region and for all bands was used as feature vector. Since there is an overlapping spectral interval in the $[650, 720]$nm region between each pair of images, a proportionality factor was applied to the *NIR* spectral curve. This factor consisted in the mean over the overlapping spectral interval of the ratios of the *VIS* and *NIR* mean (over the region of interest) signals.

Figure 2 shows the Optical Density, defined as: $OD = -\log[\frac{I_{Skin}}{I_{Spectr}}]$ (where I_{Skin} is the mean curve obtained using a robust mean technique, over all the images in the database for the same class of lesion, and I_{Spectr} is the mean curve over a region of interest of an image acquired of a spectralon) for a melanoma lesion, and for a pigmented benign lesion. Figure 3 shows the different spectral behaviour (at 650, 800 and 900nm) of a melanoma (first row) and a non melanoma (second row) lesion.

A Leave-One-Out strategy was selected (due to the low number of samples in the dataset) to create the training and testing sets formed by the feature vectors. In order to classify them, an *SVM* classifier with a Kernel Radial Basis Function (*RBF*) was used. A grid search using equally spaced steps in the logarithmic space of the *SVM tuning* parameters (C, ξ), where

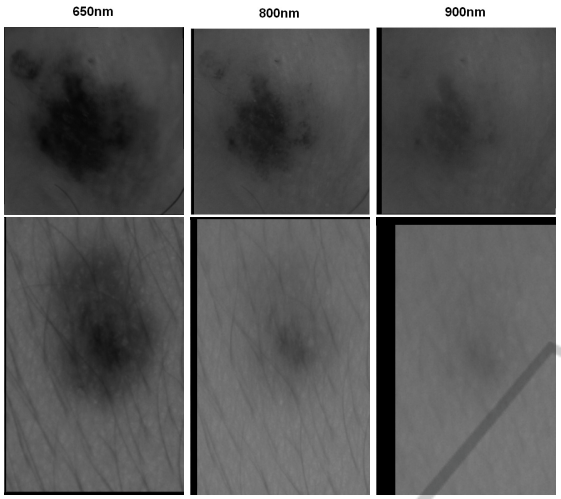

Figure 3: (First row) Spectral images of melanoma. (Second row) Spectral images of pigmented lesion, in both cases acquired at 650, 800 and 900nm.

$\xi_i = \xi, \forall i$ was made to select and fix the best parameters, using a 5-fold cross-validation strategy. In order to do a quantitative assessment of the classification *quality*, a typical two-class problem (melanoma or non-melanoma) confusion matrix as shown in Table 1 was defined. Classification results in this case are for the original dataset (without considering the class imbalance problem), where *Predicted positive* means the case when *SVM* identifies a lesion as melanoma, *Predicted negative* when *SVM* considers a lesion as non melanoma, *Positive class* when the hospital certifies the lesion is melanoma, and *Negative class* when it is not. We obtained: $TP = 1$, $TN = 17$, $FP = 3$ and $FN = 5$ (the results appear in the table as well). On the other hand, FN is probably, with TP the two most important values of the four of Table 1. $FN = 5$ in our case means that *SVM* has *let pass through* 5 melanoma lesions, without identifying them correctly. $FP = 3$ means that three lesions were wrongly identified as melanoma.

Table 1: Confusion matrix for the original dataset.

	Predicted positive	*Predicted negative*
Positive class	True Positive (TP)= 1	False Negative (FN)= 5
Negative class	False Positive (FP)= 3	True Negative (TN)= 17

With these measures, the Geometric mean (*Gm*) (Kubat and Matwin, 1997) and the Area Under the Curve (*AUC*) (Sokolova et al., 2006) were obtained. The geometric mean is defined as:

$$Gm = \sqrt{a_+ \cdot a_-} \tag{6}$$

where:

$$a_+ = \frac{TP}{TP+FN} \tag{7}$$

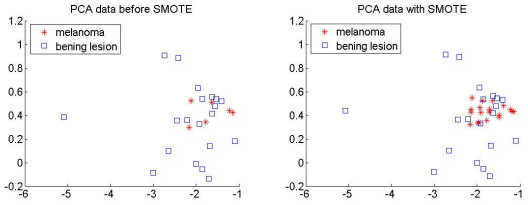

Figure 4: Plot of the first two (highest variance) *PCA* components of the spectral curves of the melanoma and non melanoma classes (left) before and (right) after applying the *SMOTE* technique.

and

$$a_- = \frac{TN}{TN+FP} \tag{8}$$

The Area Under the Curve (*AUC*) is defined as:

$$AUC = \frac{(a_+) + (a_-)}{2} \tag{9}$$

giving $Gm = 0.376$ and $AUC = 0.508$. In order to analyze the impact of the imbalance between classes on the classification performance, we applied the *SMOTE* technique on our dataset. Figure 4 shows the effect of the *SMOTE* technique on a group of points represented onto the first two components (with the highest variance) of the Principal Component Analysis (*PCA*) decomposition of the feature vectors of the melanoma and non melanoma classes of the dataset.

The generation of the synthetic prototypes in *SMOTE* was made considering $k = 3$ neighbours. Due to this random selection, the *SMOTE* technique was applied 25 times for each one of the training datasets created using the Leave-One-Out method. Since the result of the classification on each of the 25 times for each dataset could be different, a Qualified Majority Voting (*QMV*) scheme was applied. This means that a minimum percentage is required to *take a sensitive decision*. In our case, if in more than 70% of the 25 cases, the lesion were classified as non melanoma, the scheme would classify the lesion as non melanoma. In this case, the confusion matrix gives the results that appear in Table 2.

Table 2: Confusion matrix after the application of *SMOTE*.

	Predicted positive	*Predicted negative*
Positive class	True Positive (TP)= 6	False Negative (FN)= 0
Negative class	False Positive (FP)= 3	True Negative (TN)= 17

The Geometric mean (*Gm*) and the Area Under the Curve (*AUC*) gave the following results: $Gm = 0.922$ and $AUC = 0.925$. *Gm* and *AUC* results show that detection of melanoma, when applying the *SMOTE* technique, is feasible. Besides, $FN = 0$ means that the proposed technique has not *let pass through* any melanoma lesion. However, the number of False

Positives remained equal ($FP = 3$), which means that three lesions were again wrongly identified as melanoma lesions.

6 CONCLUSIONS

This paper proposes a non-invasive melanoma detection methodology based on the acquisition of multispectral images in the $[400, 1100]$nm spectral range. The classification imbalance problem inherent to this dataset was alleviated using a *SMOTE* technique. The random component of the *SMOTE* methodology was dealt with running it 25 times and a Qualified Majority Voting (*QMV*) scheme was used to do the final classification (using *SVM*). This strategy allowed to obtain good classification results ($Gm = 0.922$ and $AUC = 0.925$), as compared with the unbalanced case ($Gm = 0.376$ and $AUC = 0.508$). Also, the number of False Negatives achieved was zero ($FN = 5$ for the unbalanced case). Nevertheless, the number of False Positives was not reduced by the *SMOTE* technique. In any case, the number of samples of the dataset used is still quite low and therefore, we can only consider these as preliminary results. With more data points, future work could include the application of feature selection and texture characterization techniques.

ACKNOWLEDGEMENTS

This work was supported by the Spanish Ministry of Science and Innovation under the projects Consolider Ingenio $2010CSD2007-00018$, and EODIX $AYA\ 2008-05965-C04-04/ESP$, by the Fundació Caixa-Castelló through the project $P11B2007-48$, and by the Generalitat Valenciana through the project $PROMETEO/2010/028$.

REFERENCES

Abbasi, N. R., Shaw, H. M., and Riegel, D. S. (2004). Early diagnosis of cutaneous melanoma: revisiting the abcd criteria. *Journal of the American Medical Association*, 292:2771–2776.

Batista, G. E. A. P. A., Prati, R. C., and Monard, M. C. (2004). A study of the behavior of several methods for balancing machine learning training data. *SIGKDD Explorations Newsletter*, 6(1):20–29.

Binder, M., Kittler, H., Seeber, A., SteinerA, A., Pehamberger, H., and Wolff, K. (1998). Epiluminiscence microscopy-based classification of pigmented skin lesions using computerized image analysis and an artificial neuronal network. *Melanoma Research*, 8(3):261–266.

Carrara, M., Tomatis, S., Bono, A., Bartoli, C., Moglia, D., Lualdi, M., Colombo, A., Santinami, M., and Marchesini, R. (2005). Automated segmentation of pigmented skin lesions in multispectral imaging. *Physics in Medicine and Biology*, 50:345–357.

Chang, C. I., Q. Du, T. L. S., and Althouse, M. L. G. (1999). A joint band prioritization and band-decorrelation approach to band selection for hyperspectral image classification. *IEEE Trans. Geosc. Remote Sens.*, 37(6):2631–2641.

Chawla, N. V., Bowyer, K. W., Hall, L. O., and Kegelmeyer, W. P. (2002). SMOTE: Synthetic minority oversampling technique. *J. Artif. Intell. Res.*, 16:321–357.

Cheng, Y., Swamisai, R., Umbaugh, S. E., Moss, R. H., Stoecker, W. V., Teegala, S., and Srinivasan, S. K. (2008). Skin lesion classification using relative color features. *Skin Research and Technology*, 14:53–64.

Deshabhoina, S. V., Umbaugh, S. E., Stoecker, W. V., Moss, R. H., and Srinivasan, S. K. (2003). Melanoma and seborrheic queratosis differentiation using texture features. *Melanoma Research*, 9(4):348–356.

Dhawan, A. P., D'Alessandro, B., Patwardhan, S., and Mullani, N. (2005). An over-sampling expert system for learing from imbalanced data sets. In *Proc. of the International Conference on Neural Networks and Brain (ICNN & B '05)*, volume 1, pages 537–541.

Diebele, I., Kuzmina, I., Kapostinsh, J., Derjabo, A., and Spigulis, J. (2011). Melanoma-nevus differentiation by multispectral imaging. In *Proc. of SPIE-OSA Biomedical Optics*, volume 8087, pages 80872G1–80872G6.

ECO (2011). Cancer: Melanoma of skin. In *European Cancer Observatory http://eu-cancer.iarc.fr/cancer-11-melanoma-of-skin.html,en*.

Fernández, A., García, S., and Herrera, F. (2011). Addressing the classification with imbalanced data: Open problems and new challenges on class distribution. In Corchado, E., Kurzynski, M., and Wozniak, M., editors, *Hybrid Artificial Intelligent Systems*, volume 6678 of *Lecture Notes in Computer Science*, pages 1–10.

Friedman, R. J., Rigel, D. S., and Kopf, A. W. (1985). Early detection of malignant melanoma: the role of physician examination and self-examination of skin. *CA: A Cancer Journal for Clinicians*, 35:130–151.

He, G., Han, H., and Wang, W. (2005). An over-sampling expert system for learing from imbalanced data sets. In *Proc. of the International Conference on Neural Networks and Brain (ICNN & B '05)*, volume 1, pages 537–541.

He, H. and Garcia, E. (2009). Learning from imbalanced data. *IEEE Transactions on Knowledge and Data Engineering*, 21(9):1263–1284.

Hulse, J. V., Khoshgoftaar, T. M., and Napolitano, A. (2007). Experimental perspectives on learning from imbalanced data. In *Proc. of the 24th international conference on Machine learning (ICML'07)*, pages 935–942.

Jemal, A., Siegel, R., Xu, J., and Ward, E. (2010). Cancer statistics, 2010. *CA: A Cancer Journal for Clinicians*, 60:277–300.

Kubat, M. and Matwin, S. (1997). Addressing the curse of imbalanced training sets: one-sided selection. In *14th ICML*, pages 179–186.

Kuzmina, I., Diebele, I., Jakovels, D., Spigulis, J., Valeine, L., Kapostinsh, J., and Berzina, A. (2011a). Towards noncontact skin melanoma selection by multispectral imaging analysis. *Journal of Biomedical optics*, 16(6):0605021–0605023.

Kuzmina, I., Diebele, I., Valeine, L., Jakovels, D., Kempele, A., Kapostinsh, J., and Spigulis, J. (2011b). Multispectral imaging analysis of pigmented and vascular skin lesions: results of a clinical trial. In *Proc. of SPIE*, volume 7883, pages 7883121–7883127.

Maes, F., Collignon, A., Vandermeulen, D., Marchal, G., and Suetens, P. (1997). Multimodality image registration by maximization of mutual information. *IEEE Trans. Med. Imaging*, 16(2):187–198.

Mazzoli, A., Munaretto, R., and Scalise, L. (2010). Preliminary results on the use of a noninvasive instrument for the evaluation of the depth of pigmented skin lesions: numerical simulations and experimental measurements. *Lasers Med. Sci.*, 25:403–410.

Mogensen, M. and Jemec, G. (2007). Diagnosis of nonmelanoma skin cancer/keratinocyte carcinoma: a review of diagnostic accuracy of nonmelanoma skin cancer diagnostic tests and technologies. *Dermatol. Surg.*, 33:1158–1174.

Nagaoka, T., Nakamura, A., Okutani, H., Kiyohara, Y., and Sota, T. (2011). A possible melanoma discrimination index based on hyperspectral data: a pilot study. *Skin Research and Technology*, (DOI:10.1111/j.1600-0846.2011.00571.x):1–10.

Pluim, J. P. W., Maintz, J. B. A., and Viergever, M. A. (2003). Mutual-information-based registration of medical images: A survey. *IEEE Trans. Med. Imaging*, 22(8):986–1004.

Press, W., Teukolsky, S. A., Vetterling, W. T., and Flannery, B. P. (1992). *Numerical Recipes in C: The Art of Scientific Computing*. Cambridge University Press.

Rajaram, N., Aramil, T. J., Lee, K., Reichenberg, J. S., Nguyen, T. H., and Tunnell, J. W. (2010). Design and validation of a clinical instrument for spectral diagnosis of cutaneous malignancy. *Applied Optics*, 49(2):142–152.

Raposio, E. and et. al (2007). Spectrophotometric technology for the early detection of cutaneous melanoma. *International Journal of Simulation Systems, Science & Technology*, 8(4):46–54.

Rigel, D. S. and Friedman, R. J. (1993). The rationale of the abcds of early melanoma. *J. Am. Acadm. Dermatol.*, 29:1060–1061.

Rigel, D. S., Russak, J., and Friedman, R. (2010). The evolution of melanoma diagnosis: 25 years beyond the abcds. *CA: A Cancer Journal for Clinicians*, 60:301–316.

SCHNEIDER (2011). Industrial optics: Oem. In *http://www.schneiderkreuznach.com*.

Sokolova, M., Japkowicz, N., and Szpakowicz, S. (2006). Beyond accuracy, f-score and roc: A family of discriminant measures for performance evaluation. In Sattar, A. and Kang, B.-h., editors, *AI 2006: Advances in Artificial Intelligence*, volume 4304 of *Lecture Notes in Computer Science*, pages 1015–1021.

Sorg, B. S., Moeller, B. J., Donovan, O., Cao, Y., and Dewhirst, M. W. (2005). Hyperspectral imaging of hemoglobin saturation in tumor microvasculature and tumor hipoxia development. *Journal Biomedical Optics*, 10(4):044004.

Stanley, R. J., Stoecker, W. V., and Moss, R. H. (2007). A relative color approach to color discrimination for malignant melanoma detection in dermoscopy images. *Skin Research and Technology*, 13:62–72.

Stoecker, W. V., Wronkiewiecz, M., Chowdhury, R., Stanley, R. J., Xu, J., Bangert, A., Shrestha, B., Calcara, D. A., Rabinovitz, H. S., Oliviero, M., Ahmed, F., Perry, L. A., and Drugge, R. (2011). Detection of granularity in dermoscopy images of malignant melanoma using color and texture features. *Computerized Medical Imaging and Graphics*, 35:144–147.

Tenenhaus, A., Nkengne, A., Horn, J.-F., Serruys, C., Giron, A., and Fertil, B. (2010). Detection of melanoma from dermoscopic images of naevi acquired under uncontrolled conditions. *Skin Research and Technology*, 16:85–97.

Tomatis, S., Bono, A., Bartoli, C., Carrara, M., LualdiM, M., Tragni, G., and Marchesini, R. (2003). Automated melanoma detection, multispectral imaging and neuronal network approach for classification. *Melanoma Research*, 30(2):212–221.

Uribe, A. G., Smith, E. B., Zou, J., Duvic, M., Prieto, V., and Wang, L. V. (2011). In-vivo characterization of optical properties of pigmented skin lesions including melanoma using oblique incidence diffuse reflectance spectrometry. *Journal of Biomedical optics*, 16(2):0205011–0205013.